Journal of Solid State Chemistry 181 (2008) 2065–2072

Contents lists available at ScienceDirect

Journal of Solid State Chemistry

journal homepage: www.elsevier.com/locate/jssc

A porous open-framework titanium oxophenylphosphate

Krishanu Sarkar [a], Subhash Chandra Laha [b], Nawal Kishor Mal [c], Asim Bhaumik [a,*]

[a] Department of Materials Science and Centre for Advanced Materials, Indian Association for the Cultivation of Science, Jadavpur, Kolkata 700 032, India
[b] Institute of Chemical Technology, University of Stuttgart, D-70550 Stuttgart, Germany
[c] Catalytic Conversion and Process Development Division, Indian Institute of Petroleum, Dehradun 248 005, Uttarakhand, India

ARTICLE INFO

Article history:
Received 19 December 2007
Received in revised form
25 March 2008
Accepted 16 April 2008
Available online 3 May 2008

Keywords:
Gas adsorption
Microporous and mesoporous materials
Phenylphosphonate
Titanium phosphate

ABSTRACT

Highly porous titanium oxophenylphosphate (TPP-1) has been synthesized hydrothermally at 448 K using phenylphosphonic acid (PPA) as the organophosphorus source without the aid of any template or structure-directing agent (SDA). Powder XRD, TEM, SEM-EDS, N_2 sorption, ICP-AES chemical analysis, ^{13}C and ^{31}P MAS NMR, UV–Vis, XPS spectroscopic tools, TG-DTA and NH_3-TPD were used to characterize this material. XRD, N_2 sorption and TEM image analysis suggested the disordered layered framework structure and the presence of large-size micropores along with mesopores in this material. Spectroscopic data suggested the presence of phenyl group, O, Ti and P in this open-framework material, where Ti centers can adopt both tetrahedral and octahedral geometry. TPP-1 showed fairly good H_2 adsorption capacity under normal pressure to high pressure at 77 K. Physisorption data on hydrogen has suggested the potential application of this porous material in H_2 storage.

1. Introduction

Microporous [1,2] and mesoporous materials [3–6], which are composed of rigid inorganic frameworks and accessible internal channels and/or cages for the substrate molecules, have been the area of major research interest over the years because of their widespread applications in catalysis [7], selective adsorption [8], ion-exchange [9] and host–guest chemistry [10]. With the invention of organic–inorganic hybrid mesoporous organosilicas [11–19], the field has been further widened due to the possibility to graft a large spectrum of organic moieties inside the parent inorganic frameworks. These hybrid porous materials can be periodic solids, which can be designed to carry bulky organic functionalities [20–23]. The unique structural features of these materials make them potentially useful in a wide range of advanced applications, like chemosensor [23], environment/water cleanup [24], catalysis [25–29], photoresponsive [30,31], low-*k* dielectric [32] and magnetic measurements [33]. These new hybrid materials, as reported in the literature so far, offer well-ordered mesoporous structures, exceptionally high surface areas and surface hydrophobicity over the conventional silica-based mesostructures [3,34]. However, incidentally majority of the research works in this direction have been focused on the syntheses of silica-based mesostructures with a variety of organic functional groups and their local ordering [19,20]. There are relatively few reports on phosphate-based mesoporous hybrid materials [35–38]. In this context it is pertinent to mention that microporous phosphate-based materials containing organic functionalities are very rare. Among the phosphate-based materials, titanium oxophosphates [39] are of particular interest because of their optical and photocatalytic applications. Moreover, for the synthesis of these microporous and mesoporous materials, a single molecule template or supramolecular assembly of the surfactant molecules is essential, which can act as a structure-directing agent. Either the water structure surrounding the quaternary ammonium cations [40] or the 2D and 3D aggregated structures [3,34] can be formed by the surfactant molecules, around which a solid inorganic matrix may subsequently condense during the synthesis of these materials. Effective removal of template molecules from these composites can generate porosity in the solid materials. Since the removal of these structure-directing agent (SDA) from these materials to generate porosity is not very straightforward and so often removal of the template molecules causes collapse of the nanostructure, synthesis of microporous and mesoporous materials without the aid of any SDAs is highly desirable.

Herein, we report the synthesis of an open-framework titanium oxophenylphosphate (TPP-1) without the use of any SDA. This material showed good hydrogen adsorption capacity at 77 K. We believe that our synthetic strategy for hybrid frameworks would be widely applicable for the compositional variations of both inorganic and organic components because there is a possibility to synthesize other metal oxophenylphosphate as well as the functionalization of the aromatic ring, which could have many other potential applications.

* Corresponding author. Fax: +91 33 2473 2805.
E-mail address: msab@iacs.res.in (A. Bhaumik).

0022-4596/$ - see front matter © 2008 Elsevier Inc. All rights reserved.
doi:10.1016/j.jssc.2008.04.023

2. Experimental section

Titanium (IV) isopropoxide (97%, Aldrich) and phenylphosphonicacid (PPA, Aldrich) were used as Ti and organophosphrous sources, respectively. We have synthesized three TPP-1 samples by varying the molar ratios of Ti(i-$OC_3H_7)_4$ and C_6H_5–H_2PO_3 from 1:1 to 1:2 and 1:4, and the respective samples are designated as samples 1, 2 and 3, respectively. In a typical synthesis of sample 1, 1.59 g PPA was taken in 36 g of water and stirred for 30 min to obtain a clear aqueous solution. Then 2.84 g titanium (IV) isopropoxide was homogenized in 5 g isopropanol and this mixture was added dropwise to the above solution under vigorous stirring. After 1 h stirring, the pH of the resulting synthesis gel was ca. 6.0 and the mixture was stirred for another 2 h at room temperature. The final synthesis gel was autoclaved at 448 K for 1 day under autogenous pressure. The molar ratio of different ingredients in the final synthesis gel was

$$Ti(i-OC_3H_7)_4 : C_6H_5-H_2PO_3 : 200H_2O.$$

After the hydrothermal synthesis, the products were obtained through filtration. This was repeatedly washed with water and dried under vacuum at ambient temperature. X-ray diffraction patterns were obtained with a D8 Advance Bruker AXS SWAX diffractometer using Cu $K\alpha$ ($\lambda = 0.15406$ nm). Elemental analyses (atom emission spectrometry with inductively coupled plasma, ICP-AES) were performed on a Perkin-Elmer Plasma 400. Transmission electron microscopic images were recorded in a JEOL 2010 TEM operated at 200 kV. A JEOL JEM 6700F field emission scanning electron microscope with an EDS attachment was used to determine the morphology and chemical composition. ^{13}C CP MAS and ^{31}P MAS NMR measurements were carried out on a Bruker MSL 400 spectrometer at resonance frequencies of 100.6 and 161.92 MHz, respectively. The chemical shifts for ^{31}P spectra were referenced to orthophosphoric acid at 0 ppm. X-ray photoelectron spectrum of TPP-1 sample was recorded in a Kratos Axis ULTRA DLD X-ray photoelectron spectrometer. A low-energy electron gun with a large spot size was used for sample neutralization. The spectrum was calibrated to the C 1s peak at 285.0 eV. Nitrogen and hydrogen adsorption isotherms were obtained using a Quantachrome Autosorb 1C at 77 K. For the high-pressure H_2 gas adsorption studies, a Bel Japan Inc. Belsorp-HP was used. Prior to gas adsorption, samples were degassed for 4 h at 393 K. Thermogravimetric (TG) and differential thermal analysis (DTA) of the samples were carried out on a Perkin-Elmer DIAMOND TG/DTA instrument under N_2 flow. For the temperature programmed desorption (TPD) of ammonia, the Autosorb-1C-TCD was used. 0.2 g of the TPP-1 sample was set in a quartz cell and evacuated at 773 K for 1 h. Then ammonia gas (140 purge) was introduced into the cell and the pressure was kept for 30 min at 373 K. After these treatments, the adsorbed ammonia was desorbed in helium flow at a heating rate of 10 K min^{-1} in the temperature range 373–973 K. The amount of desorbed ammonia was analyzed by an inbuilt thermal conductivity detector (TCD) attached in the Autosorb-1C-TCD unit. Higher desorption temperature was chosen to avoid the contribution from physical adsorption of ammonia in micropores.

3. Results and discussion

3.1. Chemical analysis

Composition of different constituent elements in TPP-1 was investigated by the ICP-AES, CHN and XPS chemical analyses. XPS data suggested that the sample contained 7.38% P, 4.87% Ti and 29.15 at% of O. CHN analysis further suggested the presence of 3.7% H and 35.8 wt% of C in TPP-1. Higher at% of H could be attributed to their presence in defect P-OH sites in addition to those contributed by the adsorbed water molecules. The slight difference in the at% of H in two experiments (XPS and CHN) could be due to the different amount of absorbed water molecules as in-situ degassing is applicable in XPS only. XPS results further suggested that the atomic ratio of P/Ti was 1.51. P and Ti, determined by ICP-AES, also show similar atomic ratio (P/Ti = 1.5). This result suggested that unlike layered metal phenylphosphonates, which have a definite stoichiometry of P/metal = 2.0 in TPP-1 there are some additional Ti–O–Ti bondings. The latter could be responsible for the lower P/Ti atomic ratio in the TPP-1 material. We have derived the formula of the TPP-1 based on the chemical analysis obtained by ICP-AES, CHN, TG and XPS measurements. Based on the elemental analysis data the derived formula of the TPP-1 (without defect protons) could be represented as $Ti_{0.44}O_{0.6}(C_6H_5$–$PO_3)_{0.66}(H_2O)$, where approximately one mole of adsorbed water molecules is present in the structure.

3.2. Structural analysis by powder XRD, TEM and FE SEM

The powder X-ray diffraction patterns for the hybrid TPP-1 samples are shown in Fig. 1. As seen from the data, a single broad intense peak was observed in the low-angle diffraction patterns. The major diffraction peaks were observed at $d = 1.55$ nm with no significant wide-angle peak for either of the samples, suggesting the formation of an open-framework disordered material. The syntheses were repeated at three molar ratios of Ti(i-$OC_3H_7)_4$ and C_6H_5–H_2PO_3 (1:1, 1:2 and 1:4, Fig. 1B: a, e and c, respectively) and at three different temperatures (448, 413 and 348 K, Fig. 1B: a, d and b, respectively). Wide-angle powder XRD results for these samples are shown in Fig. 1B. It is seen from the patterns that the sample synthesized with a unimolar ratio of Ti (i-$OC_3H_7)_4$ and C_6H_5–H_2PO_3 at 448 K in the absence of any added base showed well-resolved and highly intense peaks. Thus this sample has been characterized in detail and designated as TPP-1 hereafter. This TPP-1 material is different from the layered titanium phenylphosphonate having a strong intense d_{100} peak at 1.43 nm [41]. The final pH of the synthesis gel for the TPP-1 sample was ca. pH = 6. Another sample (sample 4) has been synthesized under identical synthesis condition, where pH of the final gel was adjusted by dilute aqueous NaOH solution to *ca.* 10.0. However, the XRD intensity of this sample was very low (Fig. 1Bf). Under basic pH conditions in the presence of NaOH in the reaction medium, probably titania (TiO_2) and sodium phenylphosphanate salt were formed with no peak for the desired TPP-1 at $d = 1.55$ nm. We have heated TPP-1 at 723 K for 2 h in air and took the powder XRD pattern. TPP-1 retained its XRD pattern ($d = 1.51$ nm, not shown) after this heat treatment. This result suggested that TPP-1 retained its microstructure up to 723 K.

The TEM image of the TPP-1 is shown in Fig. 2. Low electron density spots were seen throughout the specimen. The diameter of these spots is quite uniform (*ca.* 1.0 nm). In some portions, these spots are arranged in a cross-linked linear order. This pore center to pore center correlation length could be the origin of the XRD peak at $d = 1.55$ nm. Few large spots of 2–3 nm sizes corresponding to moderate mesopores were also seen scattered in the specimen. These could be formed by the random intergrowth of the framework as seen in this image. Thus these spots suggest the existence of micropores and mesopores in this sample. However, the arrangements of these spots are not uniform throughout the specimen. The disordered feature of the material [42,43] was especially observed from the central portion of this TEM image. Thus the powder XRD and TEM results suggested that this TPP-1 has a layered framework structure with disordered mesopores.

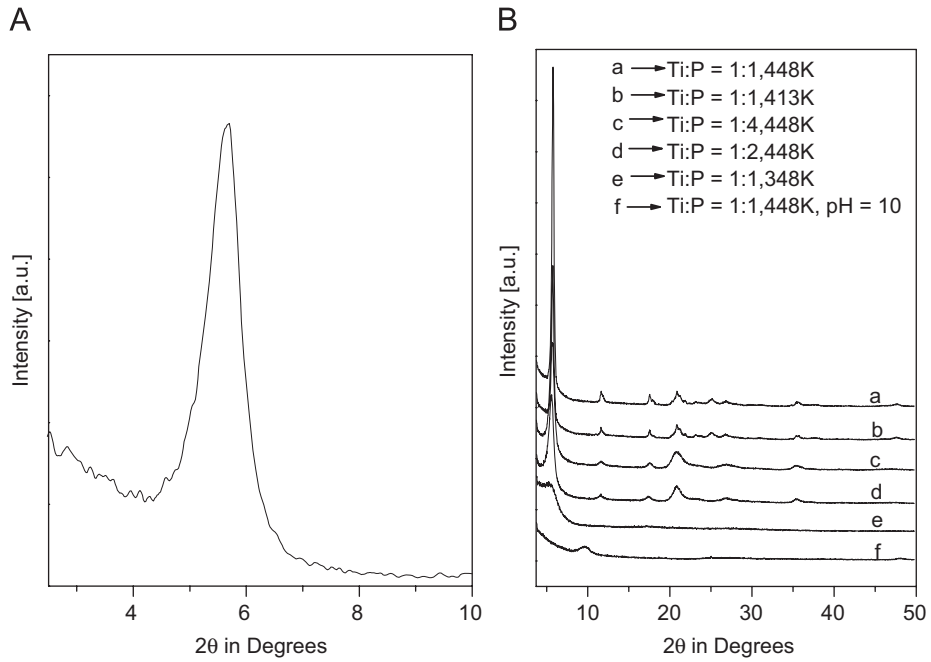

Fig. 1. Low-angle XRD pattern (A) and wide-angle patterns (B) of titanium oxophenylphosphate samples. Reaction conditions ($Ti(i\text{-}OC_3H_7)_4$: C_6H_5–H_2PO_3 mole ratio, synthesis temperatures and pH are given in the inset for each of the patterns (a–f).

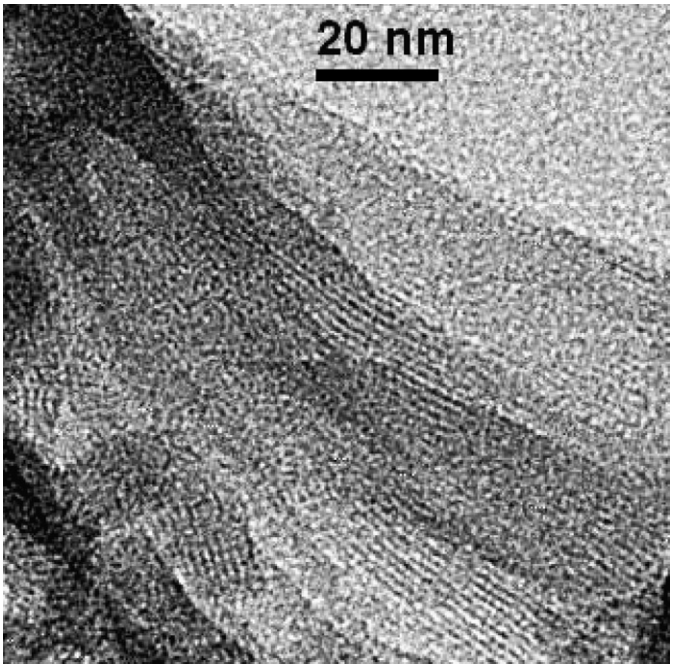

Fig. 2. Transmission electron micrograph of TPP-1.

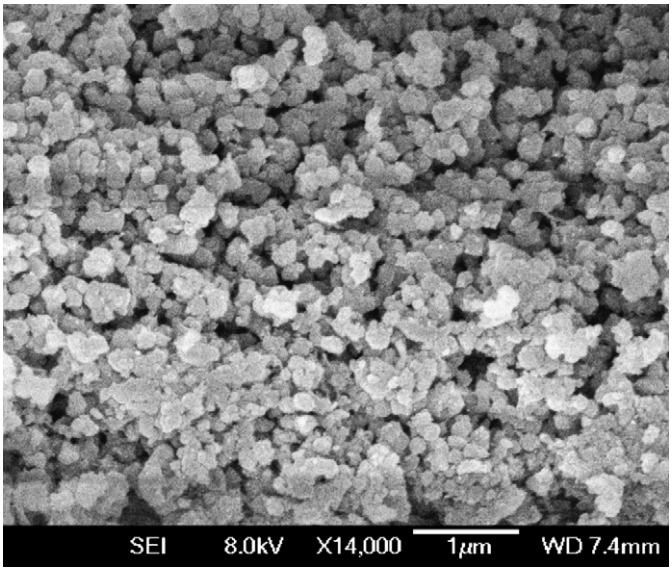

Fig. 3. SEM image of TPP-1.

FE SEM image of the hybrid TPP-1 sample (Fig. 3) suggested the formation of spherical nanoparticles of 100–200 nm dimensions. These tiny particles were found to form small spherical aggregates. Tiny particles of porous materials are particularly important from the adsorption and catalytic points of view.

3.3. Framework and bonding: ^{13}C CP MAS NMR

The ^{13}C MAS NMR spectrum of TPP-1 is shown in Fig. 4. The material exhibited two strong signals at 127.4 and 131.6 ppm. The peak at 127.4 ppm could be attributed to the C_2, C_3, C_5 and C_6 carbon atoms of the phenyl groups, whereas the peak at 131.6 ppm could be due to the C_4 atom of the phenyl group attached to the phosphonate moiety [44]. The peak due to C_1 atom of the phenyl group might have been merged along with the other signals. The observed downfield shift from the pure PPA could be due to the more confined environment in the solid matrix. This ^{13}C NMR data clearly suggested that the phenyl group in the phosphonate moiety remains intact in the hybrid TPP-1 sample.

3.4. ^{31}P MAS NMR

The ^{31}P MAS NMR spectrum of sample 1 showed a very strong and sharp signal at 13.8 ppm and a weak signal at 5.6 ppm (Fig. 5). Tetrahedral phosphorus in the neutral microporous

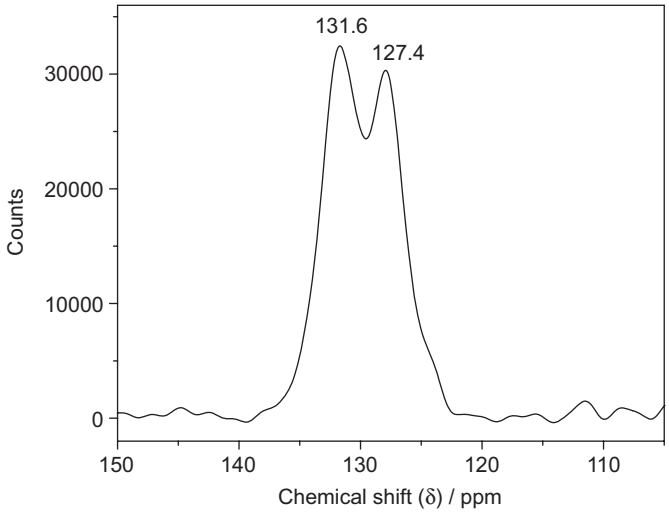

Fig. 4. ^{13}C CP MAS NMR of TPP-1.

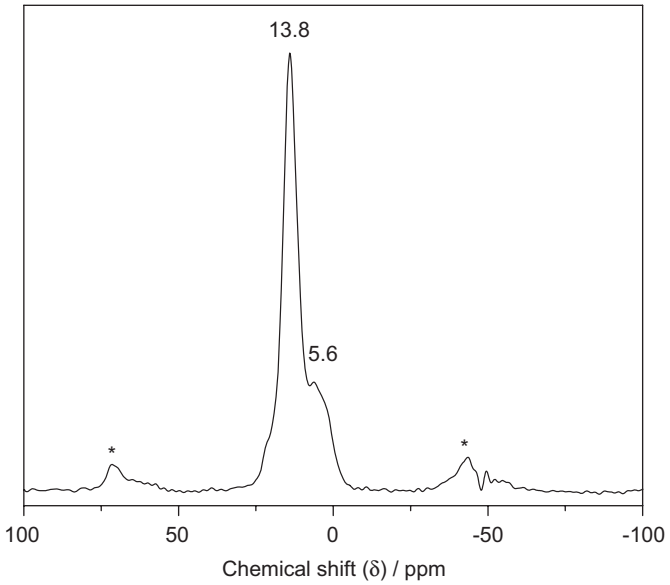

Fig. 5. ^{31}P MAS NMR spectra of TPP-1. Asterisks mark spinning side bands.

aluminophosphate materials shows a strong sharp band at around −28 to 30 ppm [45] (with respect to H_3PO_4) in the ^{31}P MAS NMR spectra, whereas signal for mesoporous titanium phosphate was observed at −5 to 3 ppm [46]. For lamellar titanium phenylphosphonates, the ^{31}P NMR chemical shifts were observed at −4 ppm [44], whereas for the hybrid xerogels composed of homogeneous dispersion of phenylphosphonate groups within a TiO_2 network show one broad signal at about 11 ppm, typical of disordered solids. Moreover, $C_6H_5P(OTi)_3$ units in molecular oxo phosphonato titanium clusters show chemical shift of 7 ppm [44]. Hence the strong peak at 13.8 ppm in TPP-1 could be due to the $C_6H_5PO_3$ species, whereas the peak at 5.6 ppm could be attributed to the $C_6H_5P(OTi)_2OH$ units in the molecular titanium oxophosphonato framework. Absence of any signal in −4 ppm ruled out the possibility of lamellar titanium phenylphosphonate impurity in the sample. High-field ^{31}P signals along with its broad feature further confirmed the presence of the phenyl group in the TPP-1 material and disordered mesostructure.

3.5. XPS for the core-level electrons

In Fig. 6, C 1*s* XPS pattern is shown. Apart from the strong peak at 285.0 eV, a broad shake-up satellite was observed for C 1*s*. This satellite structure arises conventionally for the materials containing aromatic molecules [47] where bonding π electrons are promoted to the anti-bonding π^* orbital during the photoemission process of the C 1*s* core electrons. The energy necessary for the transition is lost from the core-level peak and a satellite to low kinetic energy is observed. This broad shake-up satellites are usually observed *ca.* 6 and 10 eV higher in binding energy than the C–C peak. The photoelectron spectra of aromatic polymers usually exhibit shake-up satellites on the high binding energy side of core-level peaks [47]. The shake-up structures for the C 1*s* region (and other photoelectron peaks for O 1*s* also) from the TPP-1 indicated the presence of an aromatic phenyl group. For the P 2*p*, the observed peak position was 133.48 eV. This is characteristic of a phosphate group. In Fig. 8, Ti 2*p* photoelectron spectra are shown. Two different Ti chemical species were detected around the Ti(IV) binding energy position. The XPS measurement shows that the atomic percentage ratios for P/Ti and O/(Ti+P) were 1.51 and 2.38, respectively. The peak position for Ti $2p_{3/2}$ was 460.4 eV. Titanium (IV) atoms located at the tetrahedral positions in the titanium silicalite framework of TS-1 have Ti $2p_{3/2}$ and Ti $2p_{1/2}$ binding energies of 460 and 466 eV, respectively [48,49], whereas

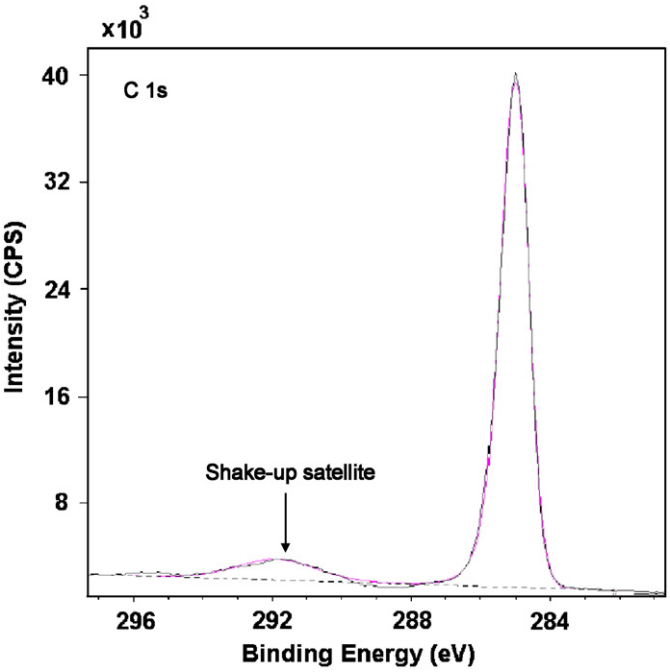

Fig. 6. XPS of C 1*s* in TPP-1.

for the octahedrally coordinated Ti (IV) attributed to extra-framework titanium atoms with a Ti $2p_{3/2}$ binding energy of 458 eV and Ti $2p_{1/2}$ of 464 eV. The presence of Ti $2p_{3/2}$ and Ti $2p_{1/2}$ peaks in our sample at 460.4 and 467.3 eV thus confirmed that a majority of the titanium species present in our sample is Ti (IV) and are tetrahedrally coordinated [7] with O in the framework. Deconvolution of this spectra (Fig. 7) suggested that out of the total Ti (IV), 67% are tetrahedrally coordinated (species I) in the framework, whereas 33% are octahedrally coordinated (species II) inside the framework. Thus the XPS results suggested that unlike the layered titanium phenylphosphonate material, where the central Ti (IV) atoms are octahedrally coordinated, TPP-1 has 2/3 of the atoms with tetrahedral coordination, whereas the remaining 1/3 are octahedrally coordinated.

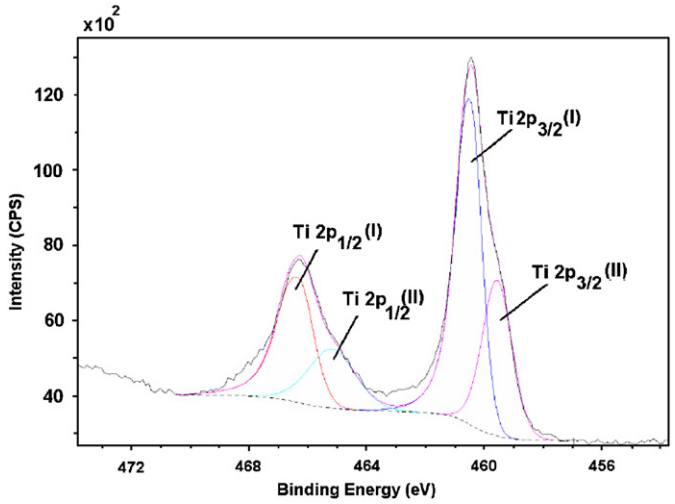

Fig. 7. XPS of Ti 2*p* in TPP-1.

3.6. Adsorption studies

3.6.1. N_2 adsorption

In Fig. 8, N_2 adsorption/desorption isotherms of TPP-1 are shown. Typical microporous materials with other chemical compositions follow similar type I isotherms at low P/P_0 regions [1]. However, at high P/P_0 (0.5–0.8) it deviates a little from the conventional type I isotherm, which is characterized by a nearly horizontal plateau into type IV isotherm. The gradual increase of N_2 uptake in this region could be attributed to the presence of mesopores and to the disordered nature of the sample [42,43]. The BET surface area for this sample was 342 $m^2 g^{-1}$. The total pore volume of TPP-1 was 0.64 $cm^3 g^{-1}$. Among this, micropore volume contributes 0.21 $cm^3 g^{-1}$. However, for the TPP-1 sample synthesized with 1:4 molar ratio of Ti(iPr)$_4$: PPA, the BET surface area and pore volume were 205 $m^2 g^{-1}$ and 0.37 $cm^3 g^{-1}$, respectively. Additional pore volume could be due to the contribution of mesopores as inferred from the nature of the isotherm. The pore diameter of the TPP-1 was estimated using the NLDFT method [50]. Here N_2 adsorption at 77 K on silica was used as the DFT kernel (cylindrical pore, NLDFT adsorption branch model). It is interesting to note that the pore size distribution as shown in the inset of Fig. 8 suggested the existence of large-size micropores and mesopores with a peak pore diameter of ca. 1.1, 2.55 and 6.0 nm, respectively. A very large range of mesopores were more pronounced in sample 3. The micropore and mesopore diameters as estimated from the N_2 sorption data agree well with the result obtained through TEM image analysis using the dimension of low electron density spots.

3.6.2. Ammonia-TPD

Fig. 9 shows the TPD-ammonia profile of TPP-1. As seen from the plot, there are two desorption peaks, a very broad one in the temperature region of 373–673 K and a sharp one in the temperature range 773–923 K. The concentration for the former one is relatively small. This peak suggested the presence of weak acid sites in the TPP-1 surface attributed to the weakly held ammonia. On the other hand, the signal observed at 873 K was very strong. Such a high desorption temperature indicated very strong acidity in the surface of the TPP-1 material. High silica zeolites having strong acid sites showed such desorption characteristics in their NH_3-TPD profile [51]. However, among phosphate-based materials strong acid sites are rare. Functionalized mesoporous silica with phosphate and titanium phosphate

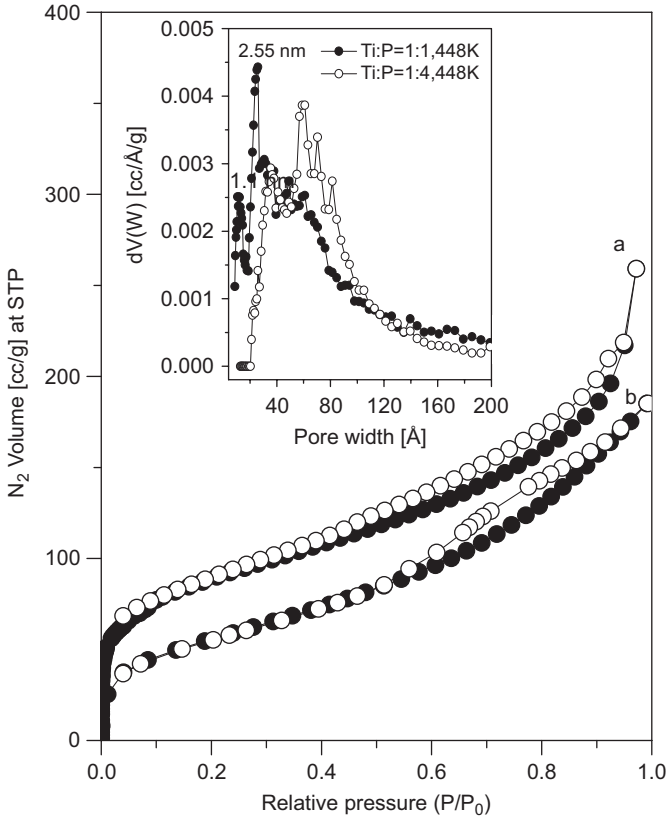

Fig. 8. N_2 adsorption/desorption isotherms of TPP-1 sample 1 (a) and 3 (b); respective pore size distribution using the NLDFT method is shown in the inset; adsorption points are marked with a filled circle, whereas that for desorption points are with open circles.

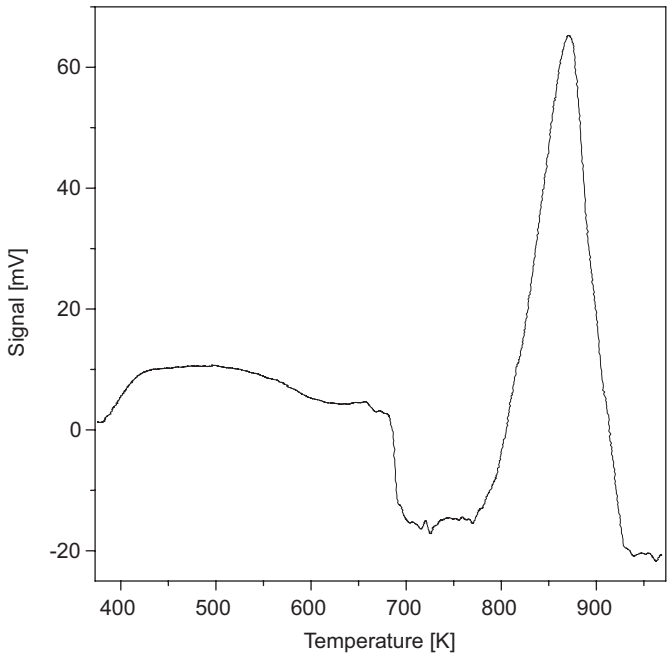

Fig. 9. Temperature-programmed desorption of ammonia over TPP-1.

groups [52] showed much lower desorption temperature and acidity than this TPP-1 material. Strength of the weak and strong acid sites was 0.42 and 1.37 mmol g^{-1}, respectively. The total strength of the acid sites was 1.79 mmol g^{-1}, which is considerably

high considering the moderate surface area of TPP-1 (342 $m^2 g^{-1}$). Thus the ammonia-TPD results revealed the presence of both weak and strong acid sites on the TPP-1 surface. Possibly there is some good degree of ionic character in the P–O–H bond (i.e. $P–O^-H^+$), which could be the origin of acid sites and adsorption of ammonia on the surface of TPP-1.

3.6.3. Thermal analysis

In Fig. 10, TGA and DTA plots for TPP-1 are shown. The sample showed weight loss of ca. 13.2% only up to 723 K in the TGA. As seen from this plot, this step is actually a combination of one sharp loss of ca. 7.0 wt% followed by a gradual decrease at elevated temperature. One small endothermic peak centered at 328 K, seen in the DTA plot, could be responsible for the first weight loss corresponding to the physically adsorbed water molecules at the surface. We could not observe any peak in the DTA plot corresponding to the gradual weight loss in the temperature range 373–723 K. This thermal analysis result suggested that the sample is stable up to 723 K without any loss of organic fragment. Above this temperature weight loss of 25.7% occurred in the temperature range 723–873 K together with a sharp endotherm at 793 K and exotherm at 823 K. These could be attributed to the C–P bond breaking and burning of phenyl groups, respectively leading to carbonized material. Since the TG analysis was carried out under N_2 flow, the whole organic mass does not decompose during this heat treatment. It has been converted into carbonized material, which accounts for 61.1 wt% residual mass even after thermal treatment at 1023 K (Fig. 10).

Lamellar phenylphosphonates of Ti and Zr have long been known to have the formula $Ti/Zr(O_3PC_6H_5)_2$ [41,53,54]. These are layered compounds with Ti or Zr atoms in the center of the plane in a near-hexagonal array. These compounds are nonporous with very poor surface areas. On the other hand, microporous tin(IV) phenylphosphonate [55,56] that derives their porosity from the aggregation of their nanosized particles have high surface areas. In our TPP-1 material microporosity and mesoporosity together with moderately good surface area were observed. XPS results suggested that unlike the 2.0 mole ratio of P/Ti and octahedral coordination in Ti(IV) in titanium phenylphosphonate [41], the TPP-1 material has a P/Ti mole ratio of 1.5 and almost 2:1 ratio of tetrahedral Ti(IV) to octahedral Ti(IV). Modified synthesis conditions employed here may be responsible for the formation of this open-framework structure of TPP-1. Based on the above results, we can say that each P atom is bonded to one phenyl group and three O atoms, whereas the Ti (IV) atoms are linked to four (for tetrahedral sites) or six (for octahedral sites) P atoms via O atoms. Phenyl groups attached with the P atoms could exist at the pore mouth as well as inside the channels. However, these phenyl groups that reside at the pore mouth could repel each other to generate void space, microporosity and mesoporosity in the framework structure. Moreover, TG analysis suggested the presence of 13.2 wt% adsorbed water in this material and ^{31}P NMR results suggested considerable defect P–OH groups at the surface. Possibly these water molecules adsorbed at the hydrophilic P–OH surfaces help to generate the void space in the framework. The orientation of the phenyl groups and the Van der Waals repulsion within the phenyl groups could direct the formation of the mesoporous structure.

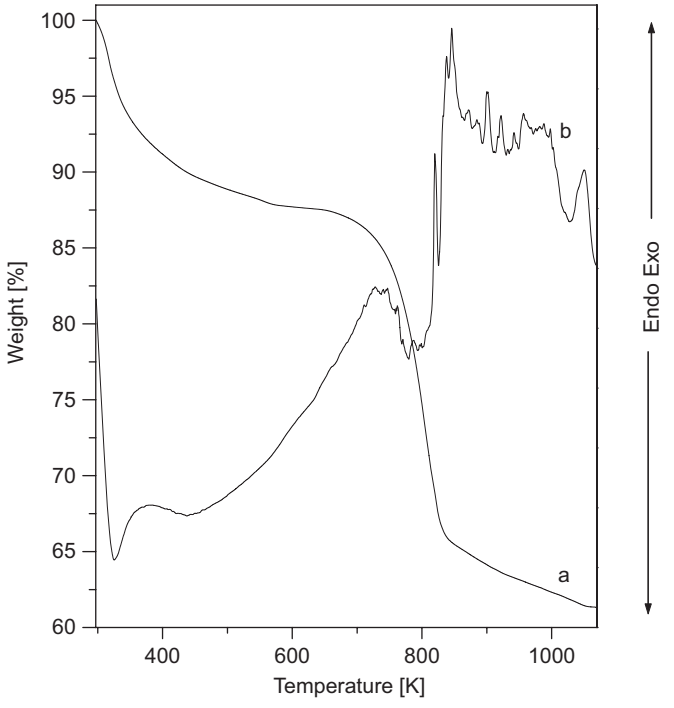

Fig. 10. TG (a) and DTA (b) plot for TPP-1.

3.6.4. H_2 storage application

In Fig. 11, the H_2 adsorption/desorption isotherms for TPP-1 (sample 1) at 77 K in the pressure range 0–1 bar are shown. From these adsorption–desorption experiments it is evident that reversible physisorption of H_2 exclusively takes place for our porous TPP-1 sample. At 1 bar atmosphere pressure of H_2 the volume adsorbed is *ca.* 42.0 $cm^3 g^{-1}$. Our N_2 sorption results suggested that TPP-1 has good surface area and pore volume. This could be responsible for the high H_2 adsorption capacity. From the nature of the isotherm, it is clear that a steady increase in the uptake of H_2 occurred with the increase in the H_2 pressure. Especially it follows an almost linear upslope near the atmospheric pressure. In Fig. 12, high-pressure H_2 adsorption isotherms for TPP-1 samples are shown. It is seen from the figure that although the initial uptake for sample 1 in the low-pressure regions was high, under high H_2 pressure uptake for sample 3 gradually peaked up. These amounts of H_2 uptake (ca. 1.0 wt% at 30 bar) are comparable with the hydrogen storage materials

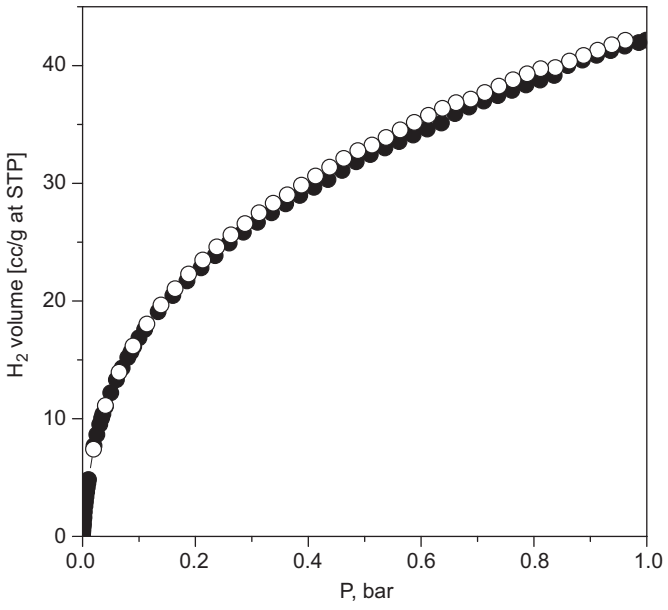

Fig. 11. H_2 adsorption/desorption isotherms on TPP-1 at 77 K; adsorption points are marked with a filled circle whereas that for desorption points are with open circles.

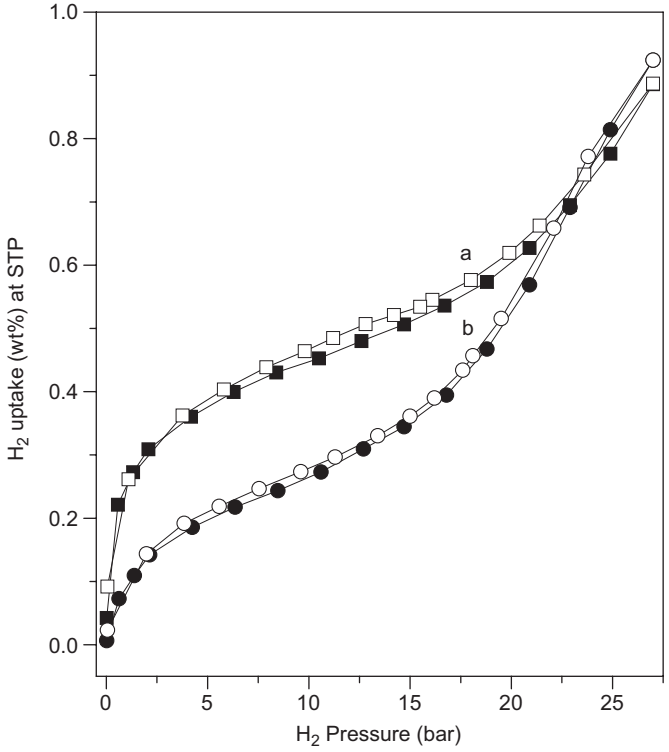

Fig. 12. High-pressure H_2 adsorption/desorption isotherms on TPP-1 samples at 77 K: sample 1 (a) and sample 3 (b). Adsorption points are marked with filled and desorption points are marked with open circles.

known in the literature [57–59]. Furthermore, these adsorption capacities did not show any trend of saturation, and the high upslope at the high-pressure region suggested that this material could find potential utility as a H_2 storage material under high applied pressure [60]. Our results demonstrate that the hydrophobic surface and void space present in this porous TPP-1 material could trap the H_2 molecules and this could be responsible for the higher hydrogen uptake.

4. Conclusions

Hybrid titanium oxophenylphosphates with large micropores and mesopores have been synthesized hydrothermally at 448 K without the use of any SDA. Powder XRD data suggested an open framework structure of the material. N_2 sorption analyses suggested the existence of medium- to large-size micropores and mesopores in the hybrid TPP-1 sample. ^{13}C, ^{31}P MAS NMR, UV–visible and XPS spectroscopic analyses suggested the presence of organic phenyl groups in this hybrid phosphate framework. XPS data further suggested that 67% of the Ti(IV) atoms are tetrahedrally coordinated whereas 33% of Ti(IV) atoms are octahedrally coordinated in the framework. High sorption capacity of H_2 under cryogenic condition suggested its utility in H_2 storage materials. The ability to graft the phenyl group in the phosphate-based molecular sieves could lead to many other potential applications of this functionalized hybrid porous solid.

Acknowledgements

K.S. thanks CSIR, New Delhi, for a junior research fellowship. A.B. wishes to thank DST, New Delhi, for a Ramanna Fellowship grant. This work was partly funded by the Nanoscience and Technology Initiative of DST. Authors wish to thank Dr. S. Hutton for the XPS measurements.

References

[1] R. Szostak, Molecular Sieves: Principles of Synthesis and Identification, Van Nostrand Reinhold, New York, 1989.
[2] A. Corma, Chem. Rev. 97 (1997) 2373.
[3] C.T. Kresge, M.E. Leonowicz, W.J. Roth, J.C. Vartuli, J.S. Beck, Nature 359 (1992) 710.
[4] P. Yang, D. Zhao, D.I. Margolese, B.F. Chmelka, G.D. Stucky, Nature 396 (1998) 152.
[5] M.G. Kanatzidis, Adv. Mater. 19 (2007) 1165.
[6] M.E. Davis, Nature 417 (2002) 813.
[7] D. Chandra, N.K. Mal, M. Mukherjee, A. Bhaumik, J. Solid State Chem. 179 (2006) 1802.
[8] J.M. Kisler, A. Dähler, A.W. Stevens, G.A.J. O'Connor, Microporous Mesoporous Mater. 44–45 (2001) 769.
[9] M.J. Manos, K. Chrissafis, M.G. Kanatzidis, J. Am. Chem. Soc. 128 (2006) 8875.
[10] E. Pardo, P. Burguete, R. Ruiz-García, M. Julve, D. Beltrán, Y. Journaux, P. Amoro's, F. Lloret, J. Mater. Chem. 16 (2006) 2702.
[11] S.L. Burkett, S.D. Simis, S. Mann, J. Chem. Soc. Chem. Commun. (1996) 1367.
[12] A. Corma, J.L. Jordá, M.T. Navarro, F. Rey, Chem. Commun. (1998) 1899.
[13] S. Inagaki, S. Guan, Y. Fukushima, T. Ohsuna, O. Terasaki, J. Am. Chem. Soc. 121 (1999) 9611.
[14] T. Asefa, M.J. MacLachlan, N. Coombs, G.A. Ozin, Nature 402 (1999) 867.
[15] B.J. Melde, B.T. Holland, C.F. Blanford, A. Stein, Chem. Mater. 11 (1999) 3302.
[16] A. Stein, B.J. Melde, R.C. Schroden, Adv. Mater. 12 (2000) 1403.
[17] A. Sayari, S. Hamoudi, Chem. Mater. 13 (2001) 3151.
[18] S. Inagaki, S. Guan, T. Ohsuna, O. Terasaki, Nature 416 (2002) 304.
[19] K. Yamamoto, T. Sakata, Y. Nohara, Y. Takahashi, T. Tatsumi, Science 300 (2003) 470.
[20] O. Olkhovyk, M. Jaroniec, J. Am. Chem. Soc. 127 (2005) 60.
[21] Y.-K. Seo, S.-B. Park, D. Ho Park, J. Solid State Chem. 179 (2006) 1285.
[22] J. Li, T. Qi, L. Wang, Y. Zhou, C. Liu, Y. Zhang, Microporous Mesoporous Mater. 103 (2007) 184.
[23] D. Chandra, T. Yokoi, T. Tatsumi, A. Bhaumik, Chem. Mater. 19 (2007) 5347.
[24] H. Yoshitake, T. Yokoi, T. Tatsumi, Chem. Mater. 14 (2002) 4603.
[25] A. Bhaumik, T. Tatsumi, J. Catal. 182 (2000) 31.
[26] A. Bhaumik, M.P. Kapoor, S. Inagaki, Chem. Commun. (2003) 470.
[27] M. Benitez, G. Bringmann, M. Dreyer, H. Garcia, H. Ihmels, M. Waidelich, K. Wissel, J. Org. Chem. 70 (2005) 2315.
[28] K. Nakajima, I. Tomita, M. Hara, S. Hayashi, K. Domen, J.N. Kondo, Adv. Mater. 17 (2005) 1839.
[29] S. Shylesh, A.P. Singh, Microporous Mesoporous Mater. 94 (2006) 127.
[30] H. Garcia, Pure Appl. Chem. 75 (2003) 1085.
[31] N.K. Mal, M. Fujiwara, T. Tanaka, Nature 421 (2003) 350.
[32] B.D. Hatton, K. Landskron, W. Whitnall, D.D. Perovic, G.A. Ozin, Adv. Funct. Mater. 15 (2005) 823.
[33] Y. Wang, C.-M. Yang, W. Schmidt, B. Spliethoff, E. Bill, F. Schüth, Adv. Mater. 17 (2005) 53.
[34] Q. Huo, D.I. Margolese, U. Ciesla, P. Feng, T.E. Gier, P. Sieger, R. Leon, P.M. Petroff, F. Schüth, G.D. Stucky, Nature 368 (1994) 317.
[35] T. Kimura, Chem. Mater. 15 (2003) 3742.
[36] W. Yan, E.W. Hagaman, S. Dai, Chem. Mater. 16 (2004) 5182.
[37] T. Kimura, Chem. Mater. 17 (2005) 337.
[38] K. Sarkar, S. Laha, A. Bhaumik, J. Mater. Chem. 16 (2006) 2438.
[39] S. Benmokhtar, H. Belmal, A.E. Jazouli, J.P. Chaminade, P. Gravereau, S. Pechev, J.C. Grenier, G. Villeneuve, D. de Waal, J. Solid State Chem. 180 (2007) 772.
[40] A.V. McCormick, A.T. Bell, Catal. Rev. 31 (1989) 97.
[41] N.K. Mal, M. Fujiwara, Y. Yamada, M. Matsukata, J. Ceram. Soc. Jpn. 111 (2003) 219.
[42] A. Bhaumik, S. Samanta, N.K. Mal, Microporous Mesoporous Mater. 68 (2004) 29.
[43] T. Sun, M.S. Wong, J.Y. Ying, Chem. Commun. (2000) 2057.
[44] G. Guerrero, P.H. Mutin, A. Vioux, Chem. Mater. 12 (2000) 1268.
[45] T. Kimura, J. Mater. Chem. 13 (2003) 3072.
[46] A. Bhaumik, S. Inagaki, J. Am. Chem. Soc. 123 (2001) 691.
[47] Y. Zhang, T. Learmonth, S. Wang, A.Y. Matsuura, J. Downes, L. Plucinski, S. Bernardis, C. O'Donnell, K.E. Smith, J. Mater. Chem. 17 (2007) 1276.
[48] D.T. On, L. Bonnevoit, A. Bittar, A. Sayari, S. Kaliaguine, J. Mol. Catal. 74 (1992) 233.
[49] Y.S.S. Wan, J.L.H. Chau, K.L. Yeung, A. Gavriilidis, J. Catal. 223 (2004) 241.
[50] A.V. Neimark, P.I. Ravikovitch, Microporous Mesoporous Mater. 44–45 (2001) 697.
[51] B. Gao, Y. Ma, Y. Cao, J. Zhao, J. Yao, J. Solid State Chem. 179 (2006) 41.
[52] N. Katada, T. Miyamoto, H. Ara Begum, N. Naito, M. Niwa, A. Matsumoto, K. Tsutsumi, J. Phys. Chem. B 104 (2000) 5511.
[53] T.V. Kovalchuk, H. Sfihi, A.S. Korchev, A.S. Kovalenko, V.G. Il'in, V.N. Zaitsev, J. Fraissard, J. Phys. Chem. B 109 (2005) 13948.
[54] G. Alberti, Acc. Chem. Res. 11 (1978) 163.
[55] N.K. Mal, M. Fujiwara, M. Matsukata, Chem. Commun. (2005) 5199.
[56] A. Subbiah, D. Pyle, A. Rowland, J. Huang, R.A. Narayanan, P. Thiyagarajan, J. Zon, A. Clearfield, J. Am. Chem. Soc. 127 (2005) 10826.

[57] L. Schlapbach, A. Zuttel, Nature 414 (2001) 353.
[58] X. Lin, J. Jia, X. Zhao, K.M. Thomas, A.J. Blake, G.S. Walker, N.R. Champness, P. Hubberstey, M. Schröder, Angew. Chem. Int. Ed. 45 (2006) 7358.
[59] P.M. Forster, J. Eckert, J.-S. Chang, S.-E. Park, G. Ferey, A.K. Cheetham, J. Am. Chem. Soc. 125 (2003) 1309.
[60] R. Gadiou, S.-E. Saadallah, T. Piquero, P. David, J. Parmentier, C. Vix-Guterl, Microporous Mesoporous Mater. 79 (2005) 121.